Journal of Magnetic Resonance 308 (2019) 106588

Contents lists available at ScienceDirect

Journal of Magnetic Resonance

journal homepage: www.elsevier.com/locate/jmr

Selective spin inversion in solution by magic field cross polarization

Joel R. Tolman [a,*,1], Luke W. Arbogast [b,1]

[a] Johns Hopkins University, Department of Chemistry, 3400 N. Charles St., Baltimore, MD 21218, United States
[b] National Institute of Standards and Technology, Institute for Bioscience and Biotechnology Research, 9600 Gudelsky Dr., Rockville, MD 20850, United States

ARTICLE INFO

Article history:
Received 20 May 2019
Revised 23 August 2019
Accepted 2 September 2019
Available online 4 September 2019

Keywords:
Cross polarization
Solution state
Spin inversion

ABSTRACT

A pulsed element is proposed allowing the selective inversion of a single ^{1}H nucleus, without regard to the presence of other degenerate ^{1}H nuclei, provided that it is coupled to a heteronuclear spin with adequate chemical shift resolution in a 2D heteronuclear correlation spectrum. The approach is based on selective cross polarization, in which matched weak RF fields of specific amplitude are applied on resonance to the targeted ^{1}H-X spin pair. It is shown theoretically that when the RF field amplitudes are set to specific values (ie. at a magic field), transfer of coherence can be fruitfully achieved transverse to the applied RF fields in addition to the normal longitudinal transfers. This enables the construction of a pulsed element which has the characteristics of a BIRD^{r,X} element (Uhrin et al., 1993), yet with 2D frequency selectivity. Demonstration of the pulsed element is made in the context of selective spin inversion, by which all ^{1}H spins are inverted except the targeted ^{1}H spin.

1. Introduction

Multidimensional NMR spectroscopy in solution relies on the ability to manipulate the quantum mechanical trajectory of the system by strategic placement of RF pulses to selectively refocus the evolution of undesirable chemical shifts and coupling interactions while allowing others to proceed [1–3]. This affords a remarkable degree of experimental control, yet the feasibility of a given application ultimately depends on the ability to apply RF pulses selectively to some spins while excluding others. As such, much effort has been directed at the development of methods for selective RF manipulation, for example by employing pulse elements to select for specific coupling topologies [4,5] or that produce the desired selective frequency response [6]. More recent developments include elegant schemes that utilize spatially selective RF to achieve broadband proton homonuclear decoupling [7,8]. Nevertheless, it remains generally difficult to discriminate between homonuclear spins that both share the same spin coupling topology and are poorly resolved in chemical shift. Further developments to achieve selective control over degenerate spins could enable novel applications to a range of systems both small and large.

Double resonance techniques can, in principle, be employed to distinguish a target spin from other degenerate spins provided that the spin of interest is coupled to a heteronuclear spin with a chemical shift that provides for adequate resolution in a 2D heteronuclear correlation spectrum. Such an approach has been previously demonstrated, in which the properties of single transition cross polarization (ST-CP) [9,10] were utilized to achieve the selective inversion of the proton in an amide ^{15}N-^{1}H spin pair in proteins [11]. However, a major limitation of that approach is that it requires a relatively long duration to execute (ca. 60 msec for an ^{15}N-^{1}H pair). Here an alternative approach is proposed based on standard cross polarization utilizing matched weak RF fields applied on resonance [12–14]. The result is a versatile pulsed element, which acts in effect as a frequency selective BIRD^{r,X} element [5], with the targeted ^{1}H-X spin pair experiencing a heteronuclear (X-spin) 180° pulse and all other non-targeted spin pairs experiencing a proton 180° pulse. When applied specifically to the problem of selective proton inversion, this element results in the inversion of all protons with the exception of the one in the ^{1}H-X spin pair targeted by the weak cross polarization (CP) fields. Significantly, this new element can be executed in a duration of $2/J_{XH}$, which for an amide ^{15}N-^{1}H or aliphatic ^{13}C–^{1}H pair corresponds to approximately 20 and 14 msec, respectively.

2. Theory

Our approach relies on exploiting differences between the quantum mechanical trajectory of a spin irradiated by just a single RF field and its trajectory when its coupled partner is simultaneously irradiated with a Hartmann-Hahn matched RF field. Cross

* Corresponding author.
E-mail address: tolman@jhu.edu (J.R. Tolman).
[1] These authors have contributed equally.

https://doi.org/10.1016/j.jmr.2019.106588
1090-7807/

polarization in liquids is generally concerned with the transfer of polarization between spins, while locked by the applied RF fields [14–16]. Provided that RF fields are strong, and Hartmann-Hahn match is achieved, this transfer is driven by just the scalar coupling part of the spin Hamiltonian. Time evolution of other components of the system will depend directly on the RF field strengths in addition to the scalar coupling J, leading to a complicated trajectory subject to both the magnitude and the associated inhomogeneity of the applied fields. If weak RF fields are employed, such that RF inhomogeneity remains small relative to J, it is possible under certain conditions to exploit more fully the evolution of the system while under CP irradiation. These specific circumstances are developed below, with a more generalized theoretical treatment placed in the Appendix A.

Expressed in the doubly rotating frame, the spin Hamiltonian for a coupled heteronuclear spin pair (IS) subjected to on resonance dual RF field irradiation is,

$$H_{CP}^{DR} = \omega_1^I I_x + \omega_1^S S_x + 2\pi J I_z S_z \tag{1}$$

where the RF fields applied to spins I and S have phase x and amplitudes producing nutation frequencies of ω_1^I and ω_1^S, respectively. As with previous descriptions of CP [14–16], it is convenient to employ zero quantum (Z) and double quantum (D) fictitious spin-1/2 operators [17], but in contrast to those treatments they are defined here relative to the untilted doubly rotating frame,

$$\begin{aligned} D_x &= \tfrac{1}{2}(I_x + S_x) & Z_x &= \tfrac{1}{2}(I_x - S_x) \\ D_y &= I_y S_z + S_y I_z & Z_y &= I_y S_z - S_y I_z \\ D_z &= I_z S_z - S_y I_y & Z_z &= I_z S_z + S_y I_y \end{aligned} \tag{2}$$

It remains that components of the operators D and Z obey the usual commutation relationships observed for an ordinary spin pair. The CP Hamiltonian of Eq. (1) becomes the following when expressed in terms of the Z and D spin operators,

$$H_{CP}^{DR} = \Sigma D_x + \Delta Z_x + \pi J D_z + \pi J Z_z \tag{3}$$

where

$$\Sigma = (\omega_1^I + \omega_1^S); \quad \Delta = (\omega_1^I - \omega_1^S) \tag{4}$$

Time evolution of the system under the CP Hamiltonian (Eq. (3)) can be visualized in terms of precession about both ZQ and DQ effective fields. The magnitude and orientation of the ZQ and DQ effective fields depends on the scalar coupling constant J and the amplitudes of the applied RF fields as shown in Fig. 1. The effective fields are inclined relative to the D_z and Z_z axes by the angles θ_D and θ_Z, respectively, and are defined formally as,

$$\begin{aligned} \theta_D &= \arctan\left(\frac{2(\nu_1^I + \nu_1^S)}{J}\right) = \arctan\left(\frac{\Sigma}{\pi J}\right) \\ \theta_Z &= \arctan\left(\frac{2(\nu_1^I - \nu_1^S)}{J}\right) = \arctan\left(\frac{\Delta}{\pi J}\right) \end{aligned} \tag{5}$$

and with corresponding magnitudes,

$$\omega_{ZQ} = \sqrt{\Delta^2 + \pi^2 J^2}; \quad \omega_{DQ} = \sqrt{\Sigma^2 + \pi^2 J^2} \tag{6}$$

In the limit of perfect Hartmann-Hahn matched RF fields applied at high power (ie. $\Sigma \gg J$) $\theta_D \approx 90°$ and $\theta_Z = 0°$. Under these circumstances the DQ effective field lies along D_x such that observed polarization transfer (longitudinal with respect to the direction of applied RF fields) occurs solely due to evolution within the ZQ manifold. At lower RF powers (with Σ comparable to J), evolution about the DQ effective field ($\theta_D < 90°$) must also be taken into account and will serve to reduce polarization transfer efficiency except at angles of precession that are a multiple of 2π. As will be discussed further below, the precessional frequencies

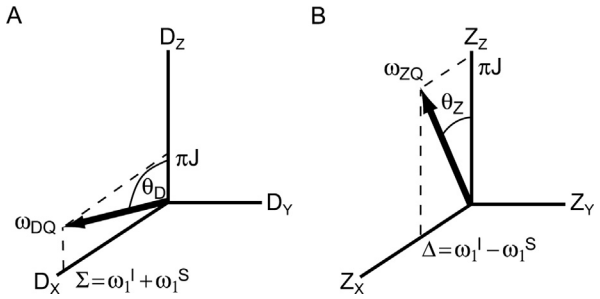

Fig. 1. Magnitude and orientation of A) DQ and B) ZQ effective fields under the on-resonance CP spin Hamiltonian within the doubly rotating frame.

about both the ZQ and DQ effective fields become of critical importance when the evolution of components of the system transverse to the applied RF is considered.

It is straightforward to calculate the time evolution of the system in a coordinate system with the z-axis oriented along the appropriate effective field (denoted as either the tilted ZQ or DQ effective field frame). Transformation of a given operator O into the tilted ZQ or DQ effective field frame (denoted with a prime) is carried out by a coordinate axis rotation about D_Y and Z_Y according to,

$$O' = T^{-1} O T \tag{7}$$

with specific rotation operators,

$$T_{DQ} = \exp\left[-i\theta_D (I_y S_z + S_y I_z)\right]; \quad T_{ZQ} = \exp\left[-i\theta_Z (I_y S_z - S_y I_z)\right] \tag{8}$$

Upon transformation into the tilted ZQ and DQ effective field frames, the CP Hamiltonian assumes a simple representation. Due to the commutativity of the Z and D operators, one can write a single composite spin Hamiltonian composed of Z and D operators each written in their own respective tilted effective field frame (specified with both a prime and applicable frame designation),

$$\begin{aligned} H_{CP}'^{ZQ/DQ} &= \omega_{ZQ} Z_{z'}^{ZQ} + \omega_{DQ} D_{z'}^{DQ} \\ &= \omega_{ZQ}\left(I_{z'}^{ZQ} S_{z'}^{ZQ} + I_{y'}^{ZQ} S_{y'}^{ZQ}\right) + \omega_{DQ}\left(I_{z'}^{DQ} S_{z'}^{DQ} - I_{y'}^{DQ} S_{y'}^{DQ}\right) \end{aligned} \tag{9}$$

Again due to commutativity of Z and D operators, the time evolution of the system in general can be calculated by accounting for precession about the ZQ and DQ effective fields in turn. Given the simple form of the CP Hamiltonian in the DQ/ZQ effective field frame (Eq. (9)), the rules governing the time evolution of a given operator A can be expressed in analogy to those utilized in the product operator formalism [18],

$$\begin{aligned} A'^{ZQ} &\xrightarrow{\omega_{ZQ} Z_{z'}^{ZQ}} A'^{ZQ}\cos(b\omega_{ZQ} t) + B'^{ZQ}\sin(b\omega_{ZQ} t); \quad ibB'^{ZQ} = \left[Z_{z'}^{ZQ}, A'^{ZQ}\right] \\ A'^{DQ} &\xrightarrow{\omega_{DQ} D_{z'}^{DQ}} AA'^{DQ}\cos(b\omega_{DQ} t) + B'^{DQ}\sin(b\omega_{DQ} t); \quad ibB'^{DQ} = \left[D_{z'}^{DQ}, A'^{DQ}\right] \end{aligned} \tag{10}$$

Note that a scalar factor, b, must be included to preserve properly normalized operators and will be reflected as a corresponding multiplicative scaling of the evolution frequencies ω_{ZQ} or ω_{DQ}. Evolution of the system with respect to both ZQ and DQ effective fields will in general result in a complex mixture of states. A special case occurs, however, when the applied RF fields are matched and set to an amplitude of

$$\omega_1^I = \omega_1^S = \pi \frac{\sqrt{(2n-1)(2n+1)}}{2} J \tag{11}$$

with n being a nonzero integer. Under these circumstances, the precessional frequencies about the ZQ and DQ effective fields become

$\omega_{ZQ} = \pi J$ and $\omega_{DQ} = 2\pi\nu J$, respectively. Setting the RF amplitudes such that they correspond to a particular value of n in Eq. (11) is referred to as the n^{th} magic field. Of primary interest is the 1st magic field setting, which is fulfilled when $\omega_1 = (2\pi) * \sqrt{3}/4 * J$. The conditions for achieving the magic field are, not by coincidence, identical to those derived by Pelupessy and Chiarparin [14] as the conditions under which evolution within the DQ manifold is fully refocused to allow for optimal polarization transfer during selective heteronuclear CP.

Expressions describing the time evolution of expectation values for specific operators under the CP Hamiltonian are obtained by transformation into the relevant tilted effective field frame, followed by calculation of the precession about that effective field, and then transformation back into the untilted doubly rotating frame (utilizing Eqs. (7), (8), and (10)). Within the ZQ and DQ manifolds, evolution will only occur with respect to the corresponding effective field. At the 1st magic field ($\theta_D = 60°$, $\theta_Z = 0°$, $\omega_{DQ} = 2\pi J$ and $\omega_{ZQ} = \pi J$), operators within the DQ manifold evolve as follows under the CP Hamiltonian,

$$\begin{bmatrix} \langle \frac{1}{2}(I_x + S_X)\rangle(t) \\ \langle I_y S_z + S_y I_z\rangle(t) \\ \langle I_z S_z - I_y S_y\rangle(t) \end{bmatrix} = \begin{bmatrix} \frac{3}{4} + \frac{1}{4}\cos(2\pi Jt) & \frac{1}{2}\sin 2\pi Jt & \frac{\sqrt{3}}{4} - \frac{\sqrt{3}}{4}\cos(2\pi Jt) \\ -\frac{1}{2}\sin 2\pi Jt & \cos 2\pi Jt & \frac{\sqrt{3}}{2}\sin 2\pi Jt \\ \frac{\sqrt{3}}{4} - \frac{\sqrt{3}}{4}\cos(2\pi Jt) & -\frac{\sqrt{3}}{2}\sin 2\pi Jt & \frac{1}{4} + \frac{3}{4}\cos(2\pi Jt) \end{bmatrix} \times \begin{bmatrix} \langle \frac{1}{2}(I_x + S_X)\rangle(0) \\ \langle I_y S_z + S_y I_z\rangle(0) \\ \langle I_z S_z - I_y S_y\rangle(0) \end{bmatrix} \tag{12}$$

Similarly for operators within the ZQ manifold,

$$\begin{bmatrix} \langle \frac{1}{2}(I_x - S_X)\rangle(t) \\ \langle I_y S_z - S_y I_z\rangle(t) \\ \langle I_z S_z + I_y S_y\rangle(t) \end{bmatrix} = \begin{bmatrix} \cos\pi Jt & \sin\pi Jt & 0 \\ -\sin\pi Jt & \cos\pi Jt & 0 \\ 0 & 0 & 1 \end{bmatrix} \begin{bmatrix} \langle \frac{1}{2}(I_x - S_X)\rangle(0) \\ \langle I_y S_z - S_y I_z\rangle(0) \\ \langle I_z S_z + I_y S_y\rangle(0) \end{bmatrix} \tag{13}$$

Evolution of operators not lying within the ZQ or DQ manifolds will precess with respect to both ZQ and DQ effective fields leading to more complicated expressions. With the exception of $2I_xS_x$, which does not evolve at all, the remaining operators can be split between two separate manifolds. Each manifold is composed of the three operators interconverted upon single field RF irradiation plus a fourth multiple quantum operator only accessible while under dual field RF irradiation. We refer to them as SQ manifolds due to the ½Σ and ½Δ ($\approx \omega_1$) frequency dependence they have with respect to each effective field and the fact that they all correspond to SQ operators when viewed in a tilted frame aligned along the direction of applied RF. As the first manifold primarily involves operators corresponding to the I spin, we refer to it as the SQ(I) manifold (specifically SQ(I) = {I_z, I_y, $2I_xS_z$, $2I_xS_y$}). It evolves under CP irradiation at the 1st magic field as follows,

The time evolution of operators within the other manifold (ie. SQ(S) = {S_z, S_y, $2S_xI_z$, $2S_xI_y$}) can be obtained from the results of Eq. (14) by simple permutation of I and S operators.

When the contact time for magic field CP irradiation is set to be $\tau_{CP} = 1/J$, useful state transformations transverse to the applied RF fields can be achieved, in addition to the normal longitudinal transfers. These transformations, expressed in the doubly rotating frame and corresponding to the spin Hamiltonian of Eq. (1), are concisely stated as,

$$\begin{aligned} &I_z \rightarrow -2I_xS_y; \quad 2I_xS_y \rightarrow I_z \\ &I_y \rightarrow 2I_xS_z; \quad 2I_xS_z \rightarrow -I_y \\ &S_z \rightarrow -2S_xI_y; \quad 2S_xI_y \rightarrow S_z \\ &S_y \rightarrow 2S_xI_z; \quad 2S_xI_z \rightarrow -S_y \\ &\tfrac{1}{2}(I_x - S_x) \rightarrow -\tfrac{1}{2}(I_x - S_x) \\ &(I_yS_z - S_yI_z) \rightarrow -(I_yS_z - S_yI_z) \end{aligned} \tag{15}$$

The remaining operators are either invariant or are restored to their initial state under magic field CP with contact time 1/J.

3. Results and discussion

The proposed pulsed element is shown in Fig. 2 and referred to as Selective Inversion by Cross Polarization (SICP). It is composed of two magic field CP elements applied for duration $1/J_{XH}$ separated by a hard 180° ^{1}H pulse, with the requirement that the ^{1}H CP field be applied with orthogonal phase to the hard pulse. We consider first the effect of the SICP element on a non-targeted ^{1}H-X spin pair where the X spin does not experience the applied X-frequency RF field. Under weak ^{1}H RF irradiation during the first τ_{CP} period, the ^{1}H spin will evolve relative to the effective field ($B_{eff} = (B_1, 0, \Delta B_0)$ with B_1 and ΔB_0 representing magnitudes of the applied ^{1}H-frequency RF field and that due to the resonance offset. Note that in the absence of an RF field experienced at the X frequency, any heteronuclear ^{1}H-X couplings present can be considered simply as additional contributions to the resonance offset field ΔB_0. As shown in previous work [11], evolution during the first τ_{CP} period about B_{eff} will be refocused during the second τ_{CP} period as a result of the intervening $(\pi)_y$ pulse. The net effect of the SICP element for non-targeted spin pairs will thus simplify to that of a ^{1}H $(\pi)_y$ pulse neglecting any corresponding losses due to spin relaxation and homonuclear coupling evolution which will remain.

For the targeted ^{1}H-X spin pair, for which both ^{1}H and X RF fields will be deliberately applied on resonance, the net effect of the SICP pulse element will be equivalent to a $(\pi)_y$ pulse applied to the X spin of the targeted spin pair. This can be shown by utilizing of the results of Eq. (15) to evaluate the net evolution over the SICP sequence. A selection of operator interconversions achieved by the SICP element is shown in Table 1 for both non-targeted

$$\begin{bmatrix} \langle I_z\rangle(t) \\ \langle I_y\rangle(t) \\ \langle 2I_xS_z\rangle(t) \\ \langle 2I_xS_y\rangle(t) \end{bmatrix} = \begin{bmatrix} \frac{3}{4}\cos(\frac{\pi}{2}Jt) & \frac{\sqrt{3}}{4}\sin(\frac{\pi}{2}Jt) & \frac{\sqrt{3}}{4}\cos(\frac{\pi}{2}Jt) & \frac{3}{4}\sin(\frac{\pi}{2}Jt) \\ +\frac{1}{4}\cos(\frac{3\pi}{2}Jt) & +\frac{\sqrt{3}}{4}\sin(\frac{3\pi}{2}Jt) & -\frac{\sqrt{3}}{4}\cos(\frac{3\pi}{2}Jt) & -\frac{1}{4}\sin(\frac{3\pi}{2}Jt) \\ -\frac{\sqrt{3}}{4}\sin(\frac{3\pi}{2}Jt) & \frac{3}{4}\cos(\frac{3\pi}{2}Jt) & \frac{3}{4}\sin(\frac{3\pi}{2}Jt) & \frac{\sqrt{3}}{4}\cos(\frac{\pi}{2}Jt) \\ -\frac{\sqrt{3}}{4}\sin(\frac{\pi}{2}Jt) & +\frac{1}{4}\cos(\frac{\pi}{2}Jt) & -\frac{1}{4}\sin(\frac{\pi}{2}Jt) & -\frac{\sqrt{3}}{4}\cos(\frac{3\pi}{2}Jt) \\ \frac{\sqrt{3}}{4}\cos(\frac{\pi}{2}Jt) & -\frac{3}{4}\sin(\frac{3\pi}{2}Jt) & \frac{3}{4}\cos(\frac{3\pi}{2}Jt) & \frac{\sqrt{3}}{4}\sin(\frac{3\pi}{2}Jt) \\ -\frac{\sqrt{3}}{4}\cos(\frac{3\pi}{2}Jt) & +\frac{1}{4}\sin(\frac{\pi}{2}Jt) & +\frac{1}{4}\cos(\frac{\pi}{2}Jt) & +\frac{\sqrt{3}}{4}\sin(\frac{\pi}{2}Jt) \\ -\frac{3}{4}\sin(\frac{\pi}{2}Jt) & \frac{\sqrt{3}}{4}\cos(\frac{\pi}{2}Jt) & -\frac{\sqrt{3}}{4}\sin(\frac{3\pi}{2}Jt) & \frac{3}{4}\cos(\frac{\pi}{2}Jt) \\ +\frac{1}{4}\sin(\frac{3\pi}{2}Jt) & -\frac{\sqrt{3}}{4}\cos(\frac{3\pi}{2}Jt) & -\frac{\sqrt{3}}{4}\sin(\frac{\pi}{2}Jt) & +\frac{1}{4}\cos(\frac{3\pi}{2}Jt) \end{bmatrix} \begin{bmatrix} \langle I_z\rangle(0) \\ \langle I_y\rangle(0) \\ \langle 2I_xS_z\rangle(0) \\ \langle 2I_xS_y\rangle(0) \end{bmatrix} \tag{14}$$

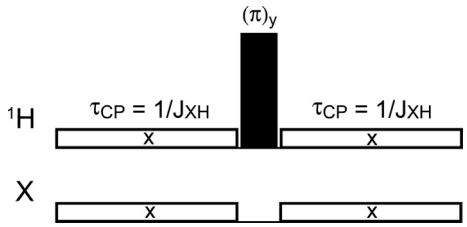

Fig. 2. The Selective Inversion by Cross Polarization (SICP) element. The open boxes represent weak RF fields which are Hartmann-Hahn matched with phase x and set to one of the magic field amplitudes (of which $\omega_1 = (2\pi) * \sqrt{3}/4 * J_{XH}$ is the smallest). The two CP contact periods are executed for a duration of $\tau_{CP} = 1/J$ and they are separated by a hard 180° y-pulse.

Table 1
Outcome of SICP for selected operators.[a]

	Final state after SICP	
Initial state	Target	Non-target
I_x	I_x	$-I_x$
I_y	I_y	I_y
I_z	I_z	$-I_z$
$2I_xS_Z$	$-2I_xS_Z$	$-2I_xS_Z$
$2I_yS_Z$	$-2I_yS_Z$	$2I_yS_Z$
$2I_zS_Z$	$-2I_zS_Z$	$-2I_zS_Z$

[a] Corresponding to a coupled I-S (^{1}H-X) spin pair.

and targeted spin pairs. It is apparent that the pathways traversed for a targeted spin pair during the SICP sequence differ substantially depending on the initial state. For example, while I_x, I_y and I_z for the targeted spin pair are all restored to their initial states by the SICP element, they respectively populate S-spin polarization (S_x), I-spin antiphase coherence ($2I_xS_z$) and multiple quantum coherence ($2I_xS_y$) after the first CP period. On the other hand, $2I_xS_z$, $2I_yS_z$ and $2I_zS_z$ states for the targeted spin pair will all be inverted and will respectively populate I-spin polarization (I_y), S-spin antiphase coherence ($2S_yI_z$) and 2-spin order ($2I_zS_z$) after the first CP period. As discussed further below, this has implications for the effects of relaxation and coupling to third spins.

An experimental demonstration of the SICP element applied to the problem of selective spin inversion was performed on a 55 mmol/L sample of D-glucose-1-^{13}C in 100% D_2O with the α-anomeric C1-H1 spin pair targeted. In this case, in which the $^1J_C{}^1H_1$ coupling constant is 170 Hz, the total duration required for the SICP element is 11.76 msec. After application of the SICP element, a 1D HSQC sequence was utilized to detect just ^{13}C-coupled protons. The RF frequency offsets in both ^{13}C and ^{1}H dimensions were systematically varied to map out the 2D frequency selectivity of the SICP element (Fig. 3). Note that the frequency selectivity is determined by the magnitude of the $^1J_{CH}$ coupling constant, with smaller coupling constants delivering greater selectivity but at the cost of longer durations to execute. We quantify the performance of the SICP element in terms of an efficiency, ε, which for spin inversion is defined as the ratio of ^{1}H Zeeman magnetization before and after application of SICP, and expressed as a percentage,

$$\varepsilon = \frac{\langle I_z \rangle_{SICP}}{\langle I_z \rangle_{t=0}} \times 100 \qquad (16)$$

In the case of spin inversion, the idealized outcome is 100% for the target spin and −100% for all other spins. For the results shown in Fig. 3, the efficiency with which the targeted magnetization was restored to the +z axis was 94%. We expect that spin relaxation and ^{1}H–^{1}H couplings (vide infra) do not contribute more than 1% each to that loss, while the remainder might reasonably be attributed to

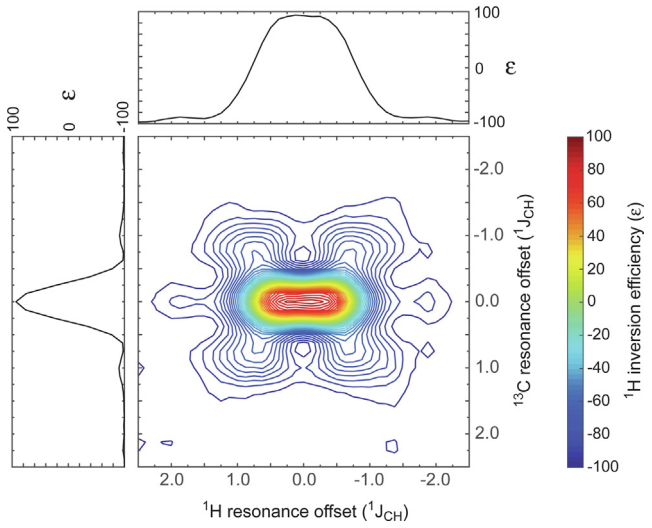

Fig. 3. Selectivity of inversion achieved with the SICP element applied at the 1st magic field settings ($\nu_1 = \omega_1/2\pi = 73.6$ Hz). Data were collected on a sample of D-glucose-1-^{13}C with the α anomeric C1-H1 spin pair targeted. The ^{1}H inversion efficiency, ε, is plotted as a function of ^{1}H and ^{13}C resonance offsets in units of $^1J_{CH}$. with resolution of 0.125 $^1J_{CH}$ (21.25 Hz).. Side panels depict 1D traces taken on resonance along ^{1}H and ^{13}C dimensions.

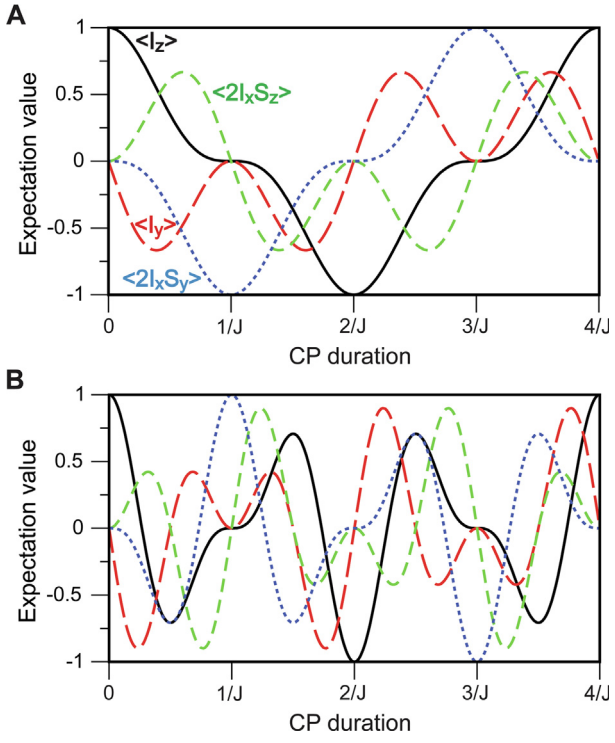

Fig. 4. Evolution of magnetization starting at ^{1}H Zeeman magnetization (I_z) for a coupled spin pair under on resonance CP irradiation with the RF fields matched and set to amplitudes at the A) first magic field ($\omega_1 = (2\pi) * \sqrt{3}/4 * J$) and the B) second magic field ($\omega_1 = (2\pi) * \sqrt{15}/4 * J$).. Note that the pure interconversion of Zeeman and multiple quantum coherence can be achieved in both cases at time 1/J. The colors and line styles are the same in both panels: I_z (black solid line), I_y (red long dashed line), $2I_xS_z$ (green dashed line), $2I_xS_y$ (blue dotted line). The reported expectation values are obtained by taking the trace over the 2-spin density matrix. (For interpretation of the references to colour in this figure legend, the reader is referred to the web version of this article.)

RF inhomogeneity of both weak and strong RF fields. The region for which there is no selectivity between spins (ie. efficiencies close to 100%) is ca. ± ½J_{CH} in the ^{1}H dimension and about half of that for

^{13}C. As can be seen, the footprint of the inversion element extends out approximately $\pm J_{CH}$ in both dimensions, with efficiencies for non-targeted spins of about −80%. Better than −90% efficiency of inversion for non-targeted spins is achieved at resonance offsets of approximately $\pm 1\frac{1}{2} J_{CH}$.

Further insights into magic field CP can be gained by considering the time evolution of the system in more detail. Shown in Fig. 4 is the simulated time evolution of relevant operators starting from pure I_z polarization followed by CP irradiation at the first and second magic field values. At the first magic field there is a monotonic decrease in I_z polarization until it reaches zero at time 1/J and this behavior is mirrored by a buildup of $2I_xS_y$, which reaches a maximum at 1/J. Transverse inphase and antiphase ^1H coherence (I_y and $2I_xS_z$, respectively) are present at intermediate times during the transfer. In contrast, a single weak ^1H RF field applied on resonance to a proton doublet leads to interconversion between I_z, I_y and $2I_xS_z$ operators (but not $2I_xS_y$). As seen in Fig. 4B, at the second magic field there is a general increase in the frequency of fluctuations of the components of the system yet very similar state outcomes are achieved at multiples of the time 1/J. At both the first and second magic fields, I_z is transformed into $2I_xS_y$ at time 1/J, but with opposite phase. Notably, the SICP element implemented at the second magic field has approximately twofold less frequency selectivity compared to results utilizing the first magic field (data not shown).

Spin relaxation effects will be especially important for large molecule applications, with details depending on the specifics of the system and the relaxation mechanisms present. In addition to potential cross-relaxation and cross-correlation effects, net losses due to spin relaxation will depend on a mixture of longitudinal, single quantum (SQ) and multiple quantum (MQ) relaxation rates. The relative contribution of each rate depends on the specific operators that evolve and thus vary greatly, as shown in Table 2. Starting from an initial state of I_z, and at the first magic field, both longitudinal ^1H relaxation and ^1H-X multiple quantum relaxation will each be operative for 31% of the time interval $\tau_{CP} = [0, 1/J]$, while ^1H inphase and antiphase single quantum relaxation rates will be operative for the remaining 38%. For comparison, during a hard 180° pulse, the system is subjected equally to longitudinal and transverse relaxation processes. We note that since the ^1H-X dipolar interaction does not contribute to the relaxation of MQ coherence, the apparent relaxation rate could be relatively favorable in cases of a spin pair lacking strong dipolar interactions to third spins. Very different circumstances accrue to cases where the initial state is I_x or I_y, in that SQ relaxation processes will be much more dominant (Table 2). Differences in apparent relaxation rates are expected at different magic fields but the effects are modest. For example, starting with I_z polarization at the second magic field, the contribution of longitudinal/MQ versus SQ relaxation rates will be 27% and 23%, respectively (compared with 31% and 19% from above).

Evolution under scalar coupling to a third spin (or more) will degrade the performance of the SICP element. Two particularly relevant scenarios are the presence of one-bond ^{13}C–^{13}C or three-bond ^1H–^1H couplings. Simulations were carried out for a pair of three spin systems with coupling topologies ^1H–^{13}C–^{13}C and ^1H..^1H–^{13}C and coupling constants $^1J_{CH} = 140$ Hz, $^1J_{CC} = 35$ Hz and $^3J_{HH} = 5$ Hz. These simulations were performed at the first three magic fields, at three different resonance offsets for the third spin, and starting from initial states of I_x, I_y and I_z. Resulting efficiencies corresponding to the targeted ^1H–^{13}C spin pair are reported in Table 3 as triplets corresponding to the starting operators I_x, I_y, and I_z. Considering the $^1J_{CC}$ case first, when the third (^{13}C) spin is on resonance the SICP element fails outright, which can be attributed to strong coupling of the ^{13}C nuclei under these conditions. When 200 Hz off resonance, SICP exhibits losses of more than 30% at the first magic field and further declines in performance at higher magic fields. We note that strong coupling effects are not negligible at this offset and the RF field strengths are of comparable magnitude to the resonance offset adding further complexity. Finally, when far enough off resonance (2000 Hz) to clearly be in a weak $^1J_{CC}$ coupling regime, at the first magic field there are losses of approximately 20% when starting from I_z or I_x but only 1% when starting from I_y. At higher magic fields these losses are all reduced to 2% or less. This is a much more dramatic reduction than one would estimate from a simple scaling down of the coupling due to a tilted effective field (from Table 3, θ_C is 63° and 71° at the 2nd and 3rd magic fields, respectively). Although the details defy simple explanation, it remains that absent strong coupling the

Table 2
Contribution to relaxation rates during SICP at 1st magic field.[a]

	Initial state		
	I_x	I_y	I_z
Longitudinal	7%	19%	31%
SQ (inphase)	55%	31%	19%
SQ (antiphase)	31%	31%	19%
MQ	7%	19%	31%

[a] Corresponding to a coupled I-S (^1H-X) spin pair.

Table 3
Effect of third spin coupling on SICP performance starting from I_x, I_y and I_z operators.

	Magic field setting		
	1st	2nd	3rd
$\omega_1/2\pi$ [Hz]	61	136	207
$\theta_{H/C}$[a]	41°	63°	71°
θ_D[b]	60°	76°	80°
ε_{CC} ($\Delta\omega/2\pi = 0$)[ce]	(14%, 14%, 1%)[f]	(1%, 17%, −2%)[f]	(−2%, 17%, −2%)[f]
ε_{CC} ($\Delta\omega/2\pi = 200$)[ce]	(69%, 96%, 67%)[f]	(79%, 73%, 55%)[f]	(68%, 53%, 28%)[f]
ε_{CC} ($\Delta\omega/2\pi = 2000$)[ce]	(80%, 99%, 79%)[f]	(99%, 99%, 98%)[f]	(99%, 99%, 98%)[f]
ε_{HH} ($\Delta\omega/2\pi = 0$)[de]	(96%, 95%, 94%)[f]	(97%, 95%, 93%)[f]	(97%, 95%, 93%)[f]
ε_{HH} ($\Delta\omega/2\pi = 200$)[de]	(99%, 99%, 99%)[f]	(99%, 99%, 98%)[f]	(99%, 98%, 97%)[f]
ε_{HH} ($\Delta\omega/2\pi = 2000$)[de]	(100%, 99%, 99%)[f]	(100%, 100%, 100%)[f]	(100%, 100%, 100%)[f]

[a] Inclination of H or C spin RF effective field from z axis when on resonance.
[b] Inclination of DQ effective field from z axis under CP dual field irradiation.
[c] Efficiency, ε_{HH}, for targeted spin pair in the presence of ^{13}C–^{13}C coupling ($^1J_{CH} = 140$ Hz; $^1J_{CC} = 35$ Hz).
[d] Efficiency, ε_{HH}, for targeted spin pair in the presence of ^1H–^1H coupling ($^1J_{CH} = 140$ Hz; $^3J_{HH} = 5$ Hz).
[e] Resonance offset, $\Delta\omega/2\pi$ [in Hz], for third coupled spin.
[f] Listed efficiencies correspond to initial states of I_x, I_y and I_z, respectively.

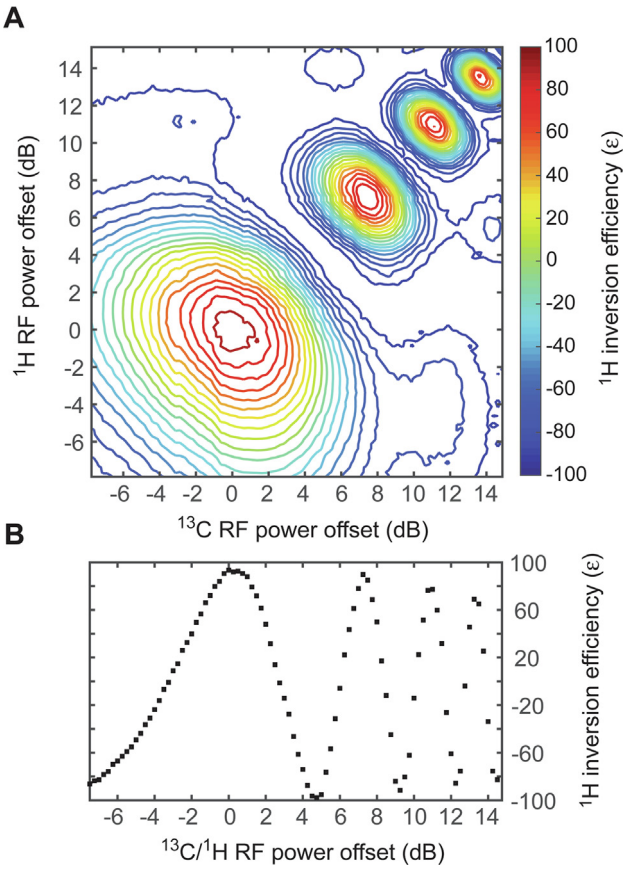

Fig. 5. Performance of SICP inversion as a function of ^{13}C and ^{1}H RF power carried out on a sample of D-glucose-1-^{13}C with the α anomeric C1-H1 spin pair targeted. A) ^{1}H inversion efficiency, ε, as a function of ^{1}H and ^{13}C RF power, acquired with a grid resolution of 0.25 dB. B) ^{1}H inversion efficiency, ε, as a function of Hartmann-Hahn matched ^{1}H and ^{13}C RF power. RF power offsets are relative to the experimentally optimized values for the 1st magic field (73.6 Hz) and correspond to RF nutation frequencies ranging from ca. 30 Hz (−7.8 dB) to 400 Hz (14.7 dB).

effects of third spin coupling are in general smaller than might be expected.

The deleterious effects of ^{1}H–^{1}H couplings are muted because of the smaller coupling constants involved and the mitigation of potential strong coupling by presence of the $^1J_{CH}$ coupling in the case investigated. Nevertheless, it remains the case that strong coupling effects do diminish SICP performance and, as for the ^{13}C–^{13}C case, the losses observed are smaller than might be expected based on simple effective field considerations. Overall we conclude that the effect of third spin ^{1}H–^{1}H couplings, while not negligible, are not likely to be important in most applications. On the other hand, larger third spin couplings such as ^{13}C–^{13}C must be considered carefully and in some cases it may be worth utilizing the 2nd magic field to mitigate the effects.

The performance of cross polarization is degraded by the presence of RF field inhomogeneity across the sample volume. The effect of inhomogeneity scales with RF field strengths and becomes important (and destructive) at magnitudes comparable to the J_{XH} coupling constant. Losses can be significant at higher RF field strengths. However, as demonstrated by Chiarparin, et al [12], polarization transfer at weak RF fields is quite insensitive to the presence of RF inhomogeneities. Here the situation is more complicated due to the requirement that the magic field be attained in addition to Hartmann-Hahn match. The results of Fig. 3, in which a total loss of 6% was observed from all sources, suggests that the SICP element is quite tolerant to RF field inhomogeneities. Further confirmation can be seen in Fig. 5A, which is a 2D contour plot of the efficiency of SICP inversion for the targeted spin as a function of ^{1}H and ^{13}C RF power utilized during the CP contact periods. At the first magic field, SICP performance can tolerate systematic variations in individual RF powers up to approximately 1 dB with corresponding loss of ca. 5% inversion efficiency from the optimal value. At variations of 2 dB RF power the corresponding loss becomes ca. 15% efficiency. This tolerance is reduced at the second magic field, where 5% and 15% efficiency losses occur at power offsets of 0.33 and 0.75 dB, respectively. As can be seen in Fig. 5B, where ^{1}H inversion efficiency is plotted vs matched RF power, optimal efficiency and insensitivity to variations in RF field strength steadily declines as one goes to higher magic fields. In practice, experimental calibration of RF power levels for the 1st magic field is slightly complicated by the broad maximum in efficiency. But by the 4th magic field the best efficiency obtainable is 70% with very steep declines observed with small adjustments in RF power levels.

4. Conclusion

It has been demonstrated that it is possible to achieve high specificity of inversion among degenerate ^{1}H spins provided that there is a coupled heteronucleus delivering sufficient 2D resolution relative to the other spin pairs. Importantly, SICP achieves a selective non– inversion in which all spins except the targeted spin is inverted. More generally, the SICP element can be considered to be a frequency selective BIRD^{r,X} [5], delivering a 180° X-pulse to the targeted ^{1}H-X spin pair and a 180° ^{1}H-pulse to all other non-targeted spin pairs. We expect it could find application in experimental contexts where the aim is to selectively perturb a coupling or NOE network, whether to facilitate measurement of parameters or even to confirm assignments. Magic field CP may find utility in other selective applications, such as seen with the recently introduced SIERRA filter, in which the magic field CP conversion of I_z into $2I_xS_y$ enables 2D frequency selective signal suppression [19]. At the low power RF fields utilized, losses due to RF inhomogeneity are on the order of a few percent using a typical solution state probe. On the other hand, couplings to third spins of sufficient magnitude can significantly compromise performance and should be carefully considered within the specific application. Although for many applications the SICP element has a manageable duration of $2/J_{XH}$, it remains that spin relaxation losses will be unacceptable for some applications. That being said, with the increase in available magnet strengths there are more applications being carried out at natural abundance or with deliberately reduced spin density, for which SICP based experimental strategies could be attractive. Finally, it must be emphasized that the SICP element is specifically designed for AX spin systems. An objective for future investigation is to develop approaches optimized for spin systems such as AX2 and AX3.

5. Methods

Certain commercial equipment, instruments, and materials are identified in this paper to specify the experimental procedure. Such identification does not imply recommendation or endorsement by the National Institute of Standards and Technology, nor does it imply that the material or equipment identified is necessarily the best available for the purpose.

5.1. NMR data acquisition and processing

All data were acquired at 25 °C on a Bruker Avance I 600 MHz spectrometer employing a room-temperature triple resonance HCN probe equipped with z-axis gradients. The SICP element was appended prior to the initial ^{1}H excitation pulse of a gradient-selected, sensitivity-enhanced ^{1}H–^{13}C HSQC experiment [20]. 1D SICP-HSQC spectra were recorded with 16 scans, a recycle delay of 1.25 s, a direct acquisition time of 100 ms over a 14 ppm spectral window, with the ^{1}H carrier set to the residual water resonance and the ^{13}C carrier set to 95 ppm. Parameter offset profiles were generated by computer-assisted parameter array in Topsin 2.1 (*popt* interface) with parameter steps of 21.25 Hz and 0.25 dB for RF carrier and field strength respectively. Data were processed with shifted sine-bell apodization prior to Fourier Transform. Spectral arrays were then read into Matlab (R2017a) as binary data to measure individual peak intensities from which respective contour plots for RF carrier and field strength offset profiles were generated.

Acknowledgements

This paper is dedicated to Prof. James H. Prestegard, a first rate scholar and mentor. We acknowledge the support of the NIST Biomanufacturing Initiative and W.M. Keck for support of the biomolecular NMR instrumentation at NIST.

Appendix A

A.1. Transformation into the tilted ZQ and DQ effective field frames

As shown in Fig. 1 and formalized in Eqs. (5), (7), and (8), the transformation into either the tilted DQ or tilted ZQ effective field frame is carried out by a coordinate frame rotation by angles of θ_D or θ_Z about the D_Y or Z_Y axes, respectively. The net effect of transformation of the CP Hamiltonian into the tilted ZQ/DQ effective field frame is to make the following substitutions,

$$\begin{aligned}
&I_zS_z - I_yS_y \overset{DQ(eff)}{\rightarrow} \left(I^{DQ}_{z'}S^{DQ}_{z'} - I^{DQ}_{y'}S^{DQ}_{y'}\right)\cos\theta_D - \tfrac{1}{2}\left(I^{DQ}_{x'} + S^{DQ}_{x'}\right)\sin\theta_D\\
&\tfrac{1}{2}(I_x + S_x) \overset{DQ(eff)}{\rightarrow} \tfrac{1}{2}\left(I^{DQ}_{x'} + S^{DQ}_{x'}\right)\cos\theta_D + \left(I^{DQ}_{z'}S^{DQ}_{z'} - I^{DQ}_{y'}S^{DQ}_{y'}\right)\sin\theta_D\\
&I_zS_z + I_yS_y \overset{ZQ(eff)}{\rightarrow} \left(I^{ZQ}_{z'}S^{ZQ}_{z'} + I^{ZQ}_{y'}S^{ZQ}_{y'}\right)\cos\theta_Z - \tfrac{1}{2}\left(I^{ZQ}_{x'} - S^{ZQ}_{x'}\right)\sin\theta_Z\\
&\tfrac{1}{2}(I_x - S_x) \overset{ZQ(eff)}{\rightarrow} \tfrac{1}{2}\left(I^{ZQ}_{x'} - S^{ZQ}_{x'}\right)\cos\theta_Z + \left(I^{ZQ}_{z'}S^{ZQ}_{z'} + I^{ZQ}_{y'}S^{ZQ}_{y'}\right)\sin\theta_Z
\end{aligned} \tag{A1}$$

The inverse transformation, taking the desired tilted effective field frame back into the doubly rotating frame, is obtained from Eq. A(1) by substitution of θ with -θ and by swapping primed and unprimed operators. The remaining transformations needed are shown in Table A1 and correspond to operators lying within the SQ(I) and SQ(S) manifolds. Notably, due to the commutation relationships of these operators with D_Y and Z_Y (=$I_yS_z \pm I_zS_y$), the operative rotation angle is just ½θ.

Table A1
Transformation of SQ(I/S) operators into tilted ZQ/DQ effective field frames.

Untitled frame	Tilted DQ effective field frame	Tilted ZQ effective field frame
I_z	$I^{DQ}_{z'}\cos\frac{1}{2}\theta_D - 2I^{DQ}_{x'}S^{DQ}_{z'}\sin\frac{1}{2}\theta_D$	$I^{ZQ}_{z'}\cos\frac{1}{2}\theta_Z - 2I^{ZQ}_{x'}S^{ZQ}_{z'}\sin\frac{1}{2}\theta_Z$
I_y	$I^{DQ}_{y'}\cos\frac{1}{2}\theta_D + 2I^{DQ}_{x'}S^{DQ}_{y'}\sin\frac{1}{2}\theta_D$	$I^{ZQ}_{y'}\cos\frac{1}{2}\theta_Z - 2I^{ZQ}_{x'}S^{ZQ}_{y'}\sin\frac{1}{2}\theta_Z$
$2I_xS_z$	$2I^{DQ}_{x'}S^{DQ}_{z'}\cos\frac{1}{2}\theta_D + I^{DQ}_{z'}\sin\frac{1}{2}\theta_D$	$2I^{ZQ}_{x'}S^{ZQ}_{z'}\cos\frac{1}{2}\theta_Z + I^{ZQ}_{z'}\sin\frac{1}{2}\theta_Z$
$2I_xS_y$	$2I^{DQ}_{x'}S^{DQ}_{y'}\cos\frac{1}{2}\theta_D - I^{DQ}_{y'}\sin\frac{1}{2}\theta_D$	$2I^{ZQ}_{x'}S^{ZQ}_{y'}\cos\frac{1}{2}\theta_Z + I^{ZQ}_{y'}\sin\frac{1}{2}\theta_Z$
S_z	$S^{DQ}_{z'}\cos\frac{1}{2}\theta_D - 2S^{DQ}_{x'}I^{DQ}_{z'}\sin\frac{1}{2}\theta_D$	$S^{ZQ}_{z'}\cos\frac{1}{2}\theta_Z - 2S^{ZQ}_{x'}I^{ZQ}_{z'}\sin\frac{1}{2}\theta_Z$
S_y	$S^{DQ}_{y'}\cos\frac{1}{2}\theta_D + 2S^{DQ}_{x'}I^{DQ}_{y'}\sin\frac{1}{2}\theta_D$	$S^{ZQ}_{y'}\cos\frac{1}{2}\theta_Z - 2S^{ZQ}_{x'}I^{ZQ}_{y'}\sin\frac{1}{2}\theta_Z$
$2S_xI_z$	$2S^{DQ}_{x'}I^{DQ}_{z'}\cos\frac{1}{2}\theta_D + S^{DQ}_{z'}\sin\frac{1}{2}\theta_D$	$2S^{ZQ}_{x'}I^{ZQ}_{z'}\cos\frac{1}{2}\theta_Z + S^{ZQ}_{z'}\sin\frac{1}{2}\theta_Z$
$2S_xI_y$	$2S^{DQ}_{x'}I^{DQ}_{y'}\cos\frac{1}{2}\theta_D - S^{DQ}_{y'}\sin\frac{1}{2}\theta_D$	$2S^{ZQ}_{x'}I^{ZQ}_{y'}\cos\frac{1}{2}\theta_Z + S^{ZQ}_{y'}\sin\frac{1}{2}\theta_Z$

A.2. Time evolution with respect to the ZQ and DQ effective fields

Calculation of the time evolution of operators within the ZQ and DQ manifolds under the CP spin Hamiltonian can be considered separately due to the fact that they commute. The mathematical description is formally identical for the ZQ and DQ manifolds, but actual system evolution normally differs substantially due to differences in the parameters θ_D and ω_{DQ} versus θ_Z and ω_{ZQ}. For the general case of arbitrary RF field strengths, evolution of operators lying within the DQ manifold is governed by,

$$\begin{bmatrix} \langle\frac{1}{2}(I_x+S_X)\rangle(t) \\ \langle I_yS_z+S_yI_z\rangle(t) \\ \langle I_zS_z-I_yS_y\rangle(t) \end{bmatrix} = \begin{bmatrix} \sin^2\theta_D & \cos\theta_D\sin\omega_{DQ}t & \sin2\theta_D\sin^2(\frac{1}{2}\omega_{DQ}t) \\ +\cos^2\theta_D\cos\omega_{DQ}t & & \\ -\cos\theta_D\sin\omega_{DQ}t & \cos\omega_{DQ}t & \sin\theta_D\sin\omega_{DQ}t \\ \sin2\theta_D\sin^2(\frac{1}{2}\omega_{DQ}t) & -\sin\theta_D\sin\omega_{DQ}t & \cos^2\theta_D \\ & & +\sin^2\theta_D\cos\omega_{DQ}t \end{bmatrix} \times \begin{bmatrix} \langle\frac{1}{2}(I_x+S_X)\rangle(0) \\ \langle I_yS_z+S_yI_z\rangle(0) \\ \langle I_zS_z-I_yS_y\rangle(0) \end{bmatrix} \tag{A2}$$

and analogously for the ZQ manifold,

$$\begin{bmatrix} \langle\frac{1}{2}(I_x-S_X)\rangle(t) \\ \langle I_yS_z-S_yI_z\rangle(t) \\ \langle I_zS_z+I_yS_y\rangle(t) \end{bmatrix} = \begin{bmatrix} \sin^2\theta_Z & \cos\theta_Z\sin\omega_{ZQ}t & \sin2\theta_Z\sin^2(\frac{1}{2}\omega_{ZQ}t) \\ +\cos^2\theta_Z\cos\omega_{ZQ}t & & \\ -\cos\theta_Z\sin\omega_{ZQ}t & \cos\omega_{ZQ}t & \sin\theta_Z\sin\omega_{ZQ}t \\ \sin2\theta_Z\sin^2(\frac{1}{2}\omega_{ZQ}t) & -\sin\theta_Z\sin\omega_{ZQ}t & \cos^2\theta_Z \\ & & +\sin^2\theta_Z\cos\omega_{ZQ}t \end{bmatrix} \times \begin{bmatrix} \langle\frac{1}{2}(I_x-S_X)\rangle(0) \\ \langle I_yS_z-S_yI_z\rangle(0) \\ \langle I_zS_z+I_yS_y\rangle(0) \end{bmatrix} \tag{A3}$$

The situation is a bit more complicated for operators within the SQ(I) and SQ(S) manifolds as their time evolution must be considered with respect to both the ZQ and DQ effective fields. This requires transformation into the tilted effective field frame first before accounting for precession about the respective effective field. Shown in Table A1 are the coordinate transformations required to carry each of these operators into the tilted DQ and ZQ effective field frames. Accounting for precession within the respective DQ and ZQ effective field frames followed by transformation back into the untilted doubly rotating frame produces the outcomes shown in Table A2.

In summary, the operators spanning the complete state space of the two spin-½ density operator can be separated into five distinct groups between which no interconversion occurs under the on resonance CP Hamiltonian (neglecting spin relaxation effects). These groups are the DQ, ZQ, SQ(I), and SQ(S) manifolds, plus the lone operator $2I_xS_x$ which does not evolve at all. Operators within the DQ and ZQ manifolds each evolve relative to their own respective effective fields while operators within the SQ(I) and SQ(S) manifolds evolve relative to both ZQ and DQ effective fields. The results for operators within the DQ and ZQ manifolds are shown in Eqs. A(2) and A(3). Final expressions for evolution of operators within the SQ manifolds under the CP Hamiltonian can be obtained from the results of Table A2. As expected, the time evolution within the SQ(I) and SQ(S) manifolds is very similar. The general result for the SQ(I) manifold is,

Table A2
Evolution of SQ(I) and SQ(S) operators relative to DQ and ZQ effective fields.

Initial operator	After DQ effective field evolution[a]	After ZQ effective field evolution[b]
I_z	$I_z\cos\phi_{DQ}$ $-(2I_xS_y\cos\theta_D + I_y\sin\theta_D)\sin\phi_{DQ}$	$I_z\cos\phi_{ZQ}$ $+(2I_xS_y\cos\theta_Z - I_y\sin\theta_Z)\sin\phi_{ZQ}$
I_y	$I_y\cos\phi_{DQ}$ $-(2I_xS_z\cos\theta_D - I_z\sin\theta_D)\sin\phi_{DQ}$	$I_y\cos\phi_{ZQ}$ $-(2I_xS_z\cos\theta_Z - I_z\sin\theta_Z)\sin\phi_{ZQ}$
$2I_xS_z$	$2I_xS_z\cos\phi_{DQ}$ $+(I_y\cos\theta_D - 2I_xS_y\sin\theta_D)\sin\phi_{DQ}$	$2I_xS_z\cos\phi_{ZQ}$ $+(I_y\cos\theta_Z + 2I_xS_y\sin\theta_Z)\sin\phi_{ZQ}$
$2I_xS_y$	$2I_xS_y\cos\phi_{DQ}$ $+(I_z\cos\theta_D + 2I_xS_z\sin\theta_D)\sin\phi_{DQ}$	$2I_xS_y\cos\phi_{ZQ}$ $-(I_z\cos\theta_Z + 2I_xS_z\sin\theta_Z)\sin\phi_{ZQ}$
S_z	$S_z\cos\phi_{DQ}$ $-(2S_xI_y\cos\theta_D + S_y\sin\theta_D)\sin\phi_{DQ}$	$S_z\cos\phi_{ZQ}$ $+(2S_xI_y\cos\theta_Z + S_y\sin\theta_Z)\sin\phi_{ZQ}$
S_y	$S_y\cos\phi_{DQ}$ $-(2S_xI_z\cos\theta_D - S_z\sin\theta_D)\sin\phi_{DQ}$	$S_y\cos\phi_{ZQ}$ $-(2S_xI_z\cos\theta_Z + S_z\sin\theta_Z)\sin\phi_{ZQ}$
$2S_xI_z$	$2S_xI_z\cos\phi_{DQ}$ $+(S_y\cos\theta_D - 2S_xI_y\sin\theta_D)\sin\phi_{DQ}$	$2S_xI_z\cos\phi_{ZQ}$ $+(S_y\cos\theta_Z - 2S_xI_y\sin\theta_Z)\sin\phi_{ZQ}$
$2S_xI_y$	$2S_xI_y\cos\phi_{DQ}$ $+(S_z\cos\theta_D + 2S_xI_z\sin\theta_D)\sin\phi_{DQ}$	$2S_xI_y\cos\phi_{ZQ}$ $-(S_z\cos\theta_Z - 2S_xI_z\sin\theta_Z)\sin\phi_{ZQ}$

[a] After system evolution for total time t with $\phi_{DQ} = \frac{1}{2}\omega_{DQ}t$.
[b] After system evolution for total time t with $\phi_{ZQ} = \frac{1}{2}\omega_{ZQ}t$.

$$\begin{bmatrix} \langle I_z\rangle(t) \\ \langle I_y\rangle(t) \\ \langle 2I_xS_z\rangle(t) \\ \langle 2I_xS_y\rangle(t) \end{bmatrix} = \begin{bmatrix} c_xc_x\cos(\frac{1}{2}\Delta\omega t) & s_xc_y\sin(\frac{1}{2}\Sigma\omega t) & s_xc_x\cos(\frac{1}{2}\Delta\omega t) & c_xc_y\sin(\frac{1}{2}\Delta\omega t) \\ +s_xs_x\cos(\frac{1}{2}\Sigma\omega t) & +c_xs_y\sin(\frac{1}{2}\Delta\omega t) & -s_xc_x\cos(\frac{1}{2}\Sigma\omega t) & -s_xs_y\sin(\frac{1}{2}\Sigma\omega t) \\ -s_xc_y\sin(\frac{1}{2}\Sigma\omega t) & c_yc_y\cos(\frac{1}{2}\Sigma\omega t) & c_xc_y\sin(\frac{1}{2}\Sigma\omega t) & s_yc_y\cos(\frac{1}{2}\Delta\omega t) \\ -c_xs_y\sin(\frac{1}{2}\Delta\omega t) & +s_ys_y\cos(\frac{1}{2}\Sigma\omega t) & -s_xs_y\sin(\frac{1}{2}\Delta\omega t) & -s_yc_y\cos(\frac{1}{2}\Sigma\omega t) \\ s_xc_x\cos(\frac{1}{2}\Delta\omega t) & -c_xc_y\sin(\frac{1}{2}\Sigma\omega t) & c_xc_x\cos(\frac{1}{2}\Sigma\omega t) & c_xs_y\sin(\frac{1}{2}\Sigma\omega t) \\ -s_xc_x\cos(\frac{1}{2}\Sigma\omega t) & +s_xs_y\sin(\frac{1}{2}\Delta\omega t) & +s_xs_x\cos(\frac{1}{2}\Delta\omega t) & +s_xc_y\sin(\frac{1}{2}\Delta\omega t) \\ -c_xc_y\sin(\frac{1}{2}\Delta\omega t) & s_yc_y\cos(\frac{1}{2}\Delta\omega t) & -c_xs_y\sin(\frac{1}{2}\Sigma\omega t) & c_yc_y\cos(\frac{1}{2}\Delta\omega t) \\ +s_xs_y\sin(\frac{1}{2}\Sigma\omega t) & -s_yc_y\cos(\frac{1}{2}\Sigma\omega t) & -s_xc_y\sin(\frac{1}{2}\Delta\omega t) & +s_ys_y\cos(\frac{1}{2}\Sigma\omega t) \end{bmatrix} \begin{bmatrix} \langle I_z\rangle(0) \\ \langle I_y\rangle(0) \\ \langle 2I_xS_z\rangle(0) \\ \langle 2I_xS_y\rangle(0) \end{bmatrix} \tag{A4}$$

while for the SQ(S) manifold it is,

$$\begin{bmatrix} \langle S_z\rangle(t) \\ \langle S_y\rangle(t) \\ \langle 2S_xI_z\rangle(t) \\ \langle 2S_xI_y\rangle(t) \end{bmatrix} = \begin{bmatrix} c_yc_y\cos(\frac{1}{2}\Delta\omega t) & s_yc_x\sin(\frac{1}{2}\Sigma\omega t) & s_yc_y\cos(\frac{1}{2}\Delta\omega t) & c_xc_y\sin(\frac{1}{2}\Delta\omega t) \\ +s_ys_y\cos(\frac{1}{2}\Sigma\omega t) & +c_ys_x\sin(\frac{1}{2}\Delta\omega t) & -s_yc_y\cos(\frac{1}{2}\Sigma\omega t) & -s_xs_y\sin(\frac{1}{2}\Sigma\omega t) \\ -s_yc_x\sin(\frac{1}{2}\Sigma\omega t) & c_xc_x\cos(\frac{1}{2}\Sigma\omega t) & c_xc_y\sin(\frac{1}{2}\Sigma\omega t) & s_xc_x\cos(\frac{1}{2}\Delta\omega t) \\ -c_ys_x\sin(\frac{1}{2}\Delta\omega t) & +s_xs_x\cos(\frac{1}{2}\Delta\omega t) & -s_xs_y\sin(\frac{1}{2}\Delta\omega t) & -s_xc_x\cos(\frac{1}{2}\Sigma\omega t) \\ s_yc_y\cos(\frac{1}{2}\Delta\omega t) & -c_xc_y\sin(\frac{1}{2}\Sigma\omega t) & c_yc_y\cos(\frac{1}{2}\Sigma\omega t) & c_ys_x\sin(\frac{1}{2}\Sigma\omega t) \\ -s_yc_y\cos(\frac{1}{2}\Sigma\omega t) & +s_xs_y\sin(\frac{1}{2}\Delta\omega t) & +s_ys_y\cos(\frac{1}{2}\Delta\omega t) & +s_yc_x\sin(\frac{1}{2}\Delta\omega t) \\ -c_xc_y\sin(\frac{1}{2}\Delta\omega t) & s_xc_x\cos(\frac{1}{2}\Delta\omega t) & -c_ys_x\sin(\frac{1}{2}\Sigma\omega t) & c_xc_x\cos(\frac{1}{2}\Delta\omega t) \\ +s_xs_y\sin(\frac{1}{2}\Sigma\omega t) & -s_xc_x\cos(\frac{1}{2}\Sigma\omega t) & -s_yc_x\sin(\frac{1}{2}\Delta\omega t) & +s_xs_x\cos(\frac{1}{2}\Sigma\omega t) \end{bmatrix} \begin{bmatrix} \langle S_z\rangle(0) \\ \langle S_y\rangle(0) \\ \langle 2S_xI_z\rangle(0) \\ \langle 2S_xI_y\rangle(0) \end{bmatrix} \tag{A5}$$

where the following abbreviations are utilized,

$$\begin{aligned} &c_x \equiv \cos x\,; \quad c_y \equiv \cos y\,; \quad s_x \equiv \sin x\,; \quad s_y \equiv \sin y \\ &\Delta\omega = (\omega_{DQ} - \omega_{ZQ})\,; \quad \Sigma\omega = (\omega_{DQ} + \omega_{ZQ}) \end{aligned} \tag{A6}$$

with mixing angles x and y defined as,

$$x = \tfrac{1}{2}(\theta_{DQ} + \theta_{ZQ}); \quad y = \tfrac{1}{2}(\theta_{DQ} - \theta_{ZQ}) \tag{A7}$$

The only difference between expressions corresponding to the SQ(I) and SQ(S) manifolds is to swap the variables x and y and spin labels I and S. Except for the signed difference between RF field magnitudes, the two spin-½ CP problem is symmetrical. As such, the results for the SQ(I) and SQ(S) manifolds are identical in the limit of Hartmann-Hahn match (where $x = y = \frac{1}{2}\theta_D$).

Useful commutators

$$\begin{aligned} &\left[2I_xS_y, I_zS_z \pm I_yS_y\right] = \pm\tfrac{1}{2}iI_z \\ &\left[I_y, I_zS_z \pm I_yS_y\right] = iI_xS_z \\ &\left[2I_xS_z, I_zS_z \pm I_yS_y\right] = -\tfrac{1}{2}iI_y \\ &\left[I_z, I_zS_z \pm I_yS_y\right] = \mp iI_xS_y \\ &\left[2I_xS_y, I_yS_z \pm I_zS_y\right] = \mp\tfrac{1}{2}iI_y \\ &\left[I_y, I_yS_z \pm I_zS_y\right] = \pm iI_xS_y \\ &\left[2I_xS_z, I_yS_z \pm I_zS_y\right] = \tfrac{1}{2}iI_z \\ &\left[I_z, I_yS_z \pm I_zS_y\right] = -iI_xS_z \end{aligned}$$

References

[1] J. Cavanagh, W.J. Fairbrother, A.G. Palmer III, N.J. Skelton, Protein NMR spectroscopy: principles and practice, Elsevier, 1995.
[2] R.R. Ernst, G. Bodenhausen, A. Wokaun, Principles of nuclear magnetic resonance in one and two dimensions, (1987).
[3] R. Freeman, Spin choreography: basic steps in high resolution NMR, Spektrum, Oxford, 1997.
[4] J.R. Garbow, D.P. Weitekamp, A. Pines, Bilinear rotation decoupling of homonuclear scalar interactions, Chem. Phys. Lett. 93 (1982) 504–509.
[5] D. Uhrin, T. Liptaj, K.E. Kover, Modified BIRD Pulses and Design of Heteronuclear Pulse Sequences, J. Magn. Reson., Ser A 101 (1993) 41–46.
[6] R. Freeman, Shaped radiofrequency pulses in high resolution NMR, Prog. Nucl. Magn. Reson. Spectrosc. 32 (1998) 59–106.
[7] L. Castañar, T. Parella, Broadband 1 H homodecoupled NMR experiments: recent developments, methods and applications, Magn. Reson. Chem. 53 (2015) 399–426.
[8] M. Foroozandeh, R.W. Adams, N.J. Meharry, D. Jeannerat, M. Nilsson, G.A. Morris, Ultrahigh-Resolution NMR Spectroscopy, Angew. Chem. Int. Ed. 53 (2014) 6990–6992.
[9] T.R. Eykyn, F. Ferrage, G. Bodenhausen, Quasi-isotropic single-transition cross-polarization in nuclear magnetic resonance, J. Chem. Phys. 116 (2002) 10041–10050.
[10] F. Fabien, R.E. Thomas, B. Geoffrey, Coherence transfer by single-transition cross-polarization: Quantitation of cross-correlation effects in nuclear magnetic resonance, J. Chem. Phys. 113 (2000) 1081–1087.
[11] L. Arbogast, A. Majumdar, J.R. Tolman, Unraveling long range residual dipolar coupling networks in strongly aligned proteins, J. Magn. Reson. 235 (2013) 26–31.
[12] E. Chiarparin, P. Pelupessy, G. Bodenhausen, Selective cross-polarization in solution state NMR, Mol. Phys. 95 (1998) 759–767.
[13] T.R. Eykyn, D.J. Philp, P.W. Kuchel, Selective cross-polarization in solution state nuclear magnetic resonance of scalar coupled spin 12 and quadrupolar nuclei, J. Chem. Phys. 118 (2003) 6997–7004.
[14] P. Pelupessy, E. Chiarparin, Hartmann-Hahn polarization transfer in liquids: An ideal tool for selective experiments, Concepts Magn. Reson. 12 (2000) 103–124.
[15] G.C. Chingas, A.N. Garroway, R.D. Bertrand, W.B. Moniz, Zero quantum NMR in the rotating frame: J cross polarization in AXN systems, J. Chem. Phys. 74 (1981) 127–156.
[16] L. Muller, R.R. Ernst, Coherence transfer in the rotating frame: application to heteronuclear cross-correlation spectroscopy, Mol. Phys. 38 (1979) 963–992.
[17] S. Vega, Fictitious spin 1/2 operator formalism for multiple quantum NMR, J. Chem. Phys. 68 (1978) 5518–5527.
[18] O.W. Sørensen, G.W. Eich, M.H. Levitt, G. Bodenhausen, R.R. Ernst, Product operator formalism for the description of NMR pulse experiments, Prog. Nucl. Magn. Reson. Spectrosc. 16 (1984) 163–192.
[19] L.W. Arbogast, F. Delaglio, J.R. Tolman, J.P. Marino, Selective suppression of excipient signals in 2D 1H–13C methyl spectra of biopharmaceutical products, J. Biomol. NMR 72 (2018) 149–161.
[20] J. Schleucher, M. Schwendinger, M. Sattler, P. Schmidt, O. Schedletzky, S.J. Glaser, O.W. Sørensen, C. Griesinger, A general enhancement scheme in heteronuclear multidimensional NMR employing pulsed field gradients, J. Biomol. NMR 4 (1994) 301–306.